environments

MDPI

Article

Quantifying Chemical-Target-Dependent Reversals in Magnetic Versus Proximity Soil-Metal Screening

Idrees F. Al-Momani [1], Mahdi S. Lataifeh [2], Emad Khaled Al-Sharadqah [1], Ghassan Malkawi [3,*], Ahmed Elsayed [4] and Haroun Albarghouthy [5]

[1] Department of Chemistry, Faculty of Science, Yarmouk University, P.O. Box 566, Irbid 21163, Jordan; imomani@yu.edu.jo (I.F.A.-M.); dr_love89@windowslive.com (E.K.A.-S.)
[2] Department of Physics, Yarmouk University, P.O. Box 566, Irbid 21163, Jordan; mahdi.q@yu.edu.jo
[3] Faculty of Computer Information Science, Higher Colleges of Technology, Al Ain P.O. Box 17155, United Arab Emirates
[4] Department of Computer Engineering and Computational Sciences, Canadian University Dubai, Dubai P.O. Box 117781, United Arab Emirates; ahmed.elsayed@cud.ac.ae
[5] Department of Mathematics and Natural Sciences, Faculty of Engineering Technology and Science, Higher Colleges of Technology, Al Ain P.O. Box 17155, United Arab Emirates; halbarghouthy@hct.ac.ae
* Correspondence: gmalkawi@hct.ac.ae

Abstract

This exploratory secondary analysis asks whether the preferred fixed-budget rule for selecting soil samples changes with the operational chemical target. Thirty-two historical surface-soil records near an iron-smelting facility in Mafraq, Jordan, contain a mass-normalized, non-independently calibrated low-frequency magnetic index (XLF), recorded factory-related distance, and four operational chemical fractions (F1, acid-soluble; F2, reducible; F3, oxidizable; and F4, modified residual) for nine elements. At equal budgets, decreasing-XLF and increasing-distance rankings were compared by retention relative to an ex post chemical optimum, enumerating cutoff ties and using uniform-random subsets as a reference. Copper was selected post hoc from the nine-element comparison as an illustrative, not confirmatory, case. At $k = 8$, XLF retained 91.7% of four-fraction Cu versus 84.7–87.6% for distance (random mean 81.8%; exact finite-subset upper-tail $p = 0.017$). For acid-soluble F1 Cu, XLF retained 84.3% versus 74.1–77.3% for distance, but its random-reference $p = 0.099$. For non-residual Cu (F1 + F2 + F3), XLF retained 60.3% versus 80.8–86.6% for distance (random mean 58.3%; XLF $p = 0.392$). These fixed-record comparisons do not establish contamination, bioavailability, source attribution, or transferable predictive accuracy. Screening performance must be evaluated for the intended chemical fraction and against a chance reference.

Keywords: magnetic susceptibility; sequential extraction; copper; soil metals; screening design

Check for updates

Academic Editor: Ioannis K. Kalavrouziotis

Received: 5 October 2026
Revised: 10 November 2026
Accepted: 10 November 2026
Published: 15 November 2026

Copyright: © 2026 by the authors. Licensee MDPI, Basel, Switzerland. This article is an open access article distributed under the terms and conditions of the Creative Commons Attribution (CC BY) license.

1. Introduction

Low-frequency magnetic susceptibility is used for environmental pre-screening because measurement is rapid and non-destructive relative to multi-element chemical analysis. The archived study variable XLF is a mass-normalized numerical index whose physical susceptibility scale is not independently calibrated (Section 2.2). Studies in industrial soils, urban soils, sediments, and metallurgical settings have repeatedly shown that magnetic enrichment can co-occur with elevated concentrations of potentially toxic elements [1–6]. However, the strength and direction of these relationships are site-specific because mag-

netic signals respond to mineralogy, particle sources, grain size, pedogenic processes, and industrial inputs rather than to metal concentration alone.

A second, less explicit limitation is that "metal contamination" is not a single chemical target. Sequential extraction separates operational pools with different extractabilities. A site that ranks highly by the sum of sequentially extracted fractions may not rank highly by the acid-soluble first fraction or by the combined non-residual fractions. Work combining magnetic measurements with fractionation has shown that relationships between magnetic susceptibility and metals can differ among chemical fractions [7]. This creates a practical monitoring question that is distinct from ordinary correlation: if only a limited number of locations can be prioritized for chemical follow-up, does a magnetic ranking recover the same chemically important records when the target changes?

The historical chemistry originates from the 2015 master's thesis by co-author Emad Khaled Al-Sharadqah, *Sequential Fractionation of Heavy Metals in Soils around the Iron Smelting Factory in Mafraq, Jordan*, supervised by Idrees F. Al-Momani at Yarmouk University [8]. The thesis investigated nine elements in 32 surface-soil samples and four ash samples, using acid digestion, sequential extraction, and flame atomic absorption spectrometry (FAAS). It compared concentrations and operational fractions inside and outside the factory and examined spatial differences. Tables 3.5 and 3.6 of that 2015 thesis reported residual Cu shares of 62.0% and 75.5% for the inside and outside groups, respectively. These are historical thesis summaries, not new estimates from the present reanalysis. The extraction stages, inconsistencies in the historical quality-control table, and unresolved sampling-month discrepancy are described in Section 2.1 and Supplementary File S1.

The present secondary analysis asks a different question: when the same number of records can be selected for chemical follow-up, does the preferred rule—higher XLF or shorter factory-center distance—change with the chemical target? The 32-record analytical table links the soil chemistry to magnetic readings, specimen mass, coordinates, distance, and direction. A separate historical magnetic worksheet cross-checks record identity; it does not add independent samples. The contribution is a target-dependent reversal in a fixed-record decision comparison, not a new field survey, a new extraction procedure, or a general claim that susceptibility detects individual metals. Spatial context remains relevant: proximity and wind direction can structure contamination around industrial facilities [9], and magnetic mapping can guide chemical sampling [10,11]. Here, recorded distance from the factory center is a simple comparator, not a dispersion model. Cd, Pb, and Zn can co-occur with magnetic assemblages without being directly detected by susceptibility.

Magnetic pre-screening itself is established: Cao et al. [12] quantified the efficiency of targeted chemical sampling after magnetic mapping, while Wang et al. [7] and Ye et al. [13] showed that magnetic–metal relationships can depend on chemical fraction or operational availability. The unresolved decision question is whether a ranking that performs well for one chemical target remains useful when the target changes within the same element. The objectives are to compare decreasing XLF with increasing distance from the factory center across all nine elements and three operational targets at equal budgets, assess performance against uniform selection of the same number of records, and test sensitivity to alternative magnetic variables, record order, and provenance. The descriptive hypothesis is that the rule ordering changes with the chemical target; it was not preregistered. Cu was chosen post hoc as the clearest illustrative target reversal. A strict winner in the pairwise comparison is not necessarily better than chance, nor is it an inferentially validated screening method.

2. Materials and Methods

2.1. Historical Study and Analytical Provenance

The thesis [8] describes the Chinese Iron Smelting Factory in Mafraq, northern Jordan, as processing scrap iron in large electrical furnaces with water-spray filters in its chimneys. This description concerns the historical study period, not present operations or quantified emissions. Figure 1 locates the study area within Jordan and displays the 32 archived record coordinates. The national outline is generalized cartographic context [14]; no factory boundary, land-use classification, or emissions footprint is inferred. Here, "factory-center distance" is a descriptive name for the column labeled `distance(m)` in the archived workbook. The historical record does not establish an independently surveyed measurement origin, production-stack location, or geometric factory center.

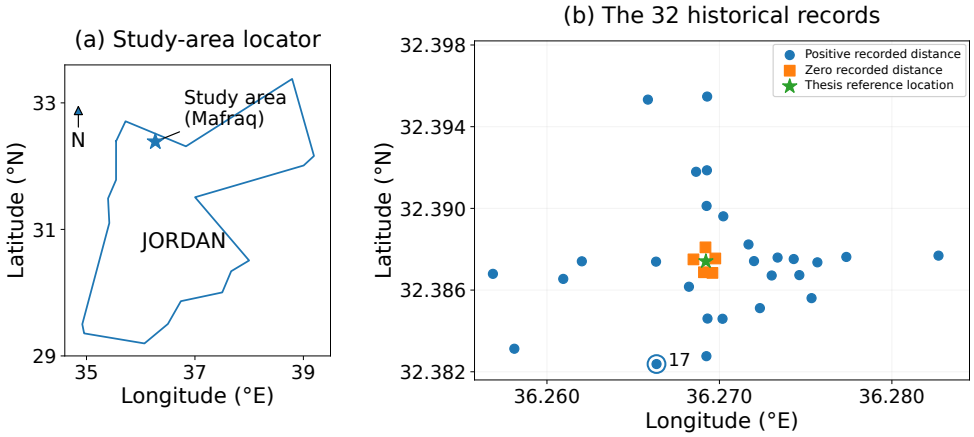


Figure 1. Study-area location and archived soil-record coordinates. (**a**) Generalized Jordan outline from Natural Earth; the marker uses the approximate study-area coordinate stated in the 2015 thesis. (**b**) All 32 record coordinates were converted from the archived degree–minute–second entries to decimal degrees. Squares mark the five records with distance coded zero; record 17 is ringed. Only record 17 is labeled to avoid overlapping labels in the central cluster. The label N indicates north. The star is the thesis reference location, not an independently surveyed factory center. Axes show geographic coordinates; source datum and positional accuracy were not independently documented. The figure is not a surveyed factory boundary, a reconstructed emissions map, or a new field measurement.

The 32 soil records (plus four separate ash samples not used here) were collected at 0–15 cm. Soil was air-dried, crushed, and passed through a 250 µm sieve. The historical procedure is described here as Community Bureau of Reference (BCR)-based sequential extraction with modified residual digestion; equivalence to every reference-protocol condition is not established. The contemporaneous thesis, however, explicitly labels the subsequent residual stage "Residual Fraction (Modified)"; accordingly, the complete four-fraction sequence is not described as an unmodified four-step BCR standard. For each 1 g aliquot, F1 used 40 mL of 0.11 M acetic acid to extract relatively acid-soluble/exchangeable and carbonate-associated material; F2 used 40 mL of 0.5 M hydroxylamine hydrochloride at pH 1.5 to target reducible oxide-associated material; and F3 involved hydrogen-peroxide oxidation followed by 1 M ammonium acetate at pH 2 for oxidizable material. The remaining residue was subjected to an additional strong-acid microwave digestion for F4, as specified in the thesis; this fourth stage is distinct from the three-stage BCR extraction [15]. The thesis reports 40 mL ammonium acetate in F3 and centrifugation at 3000 rpm, whereas the BCR-701 reference procedure specifies 50 mL and a relative centrifugal force of 3000× *g* [16]. The source values are retained: rotor radius and complete shaking-duration records are unavailable, so missing conditions are not inferred from the reference procedure (Supplementary File S1, Section S20). The 1 g chemical aliquot is distinct from the

specimen mass used for magnetic measurement. These reagent choices intentionally probe different operational pools; the mild first extraction is not a substitute for strong-acid total digestion. Fractions are not unique mineral phases, environmental mobility measurements, or bioavailability estimates [15,17,18].

Nine elements (Cd, Co, Cr, Cu, Fe, Mn, Ni, Pb and Zn) were measured using FAAS on the historical extracts. The thesis reports quality assurance/quality control (QA/QC) through blanks, blank correction, calibration and solution detection-limit procedures, using two National Institute of Standards and Technology (NIST) standard reference materials (SRMs) described in its text as 1646a and 2702. These SRMs were microwave-digested, not reported as subjected to the full sequential-extraction stages. Moreover, Table 2.3 of the 2015 thesis reports heterogeneous measured-to-listed-reference ratios: for Cd in the first SRM, $0.63/0.15 = 4.20$ (420%), whereas for Cu in the same SRM, $9.90/10.01 \approx 0.989$; in the second SRM, Mn is $1405/1757 \approx 0.800$. Its first-SRM heading ("1664a") conflicts with the text ("1646a"), and the second-SRM certified Cu entry is blank. These are checks on the reported historical QA/QC table, not independent certificate verification or correction of the archived chemistry. No use of BCR-701 or another dedicated fraction-specific certified reference material (CRM) is documented in the available sources; fraction-by-fraction extraction recovery therefore remains unverified. The available source also does not map any individual spreadsheet value to the original solution detection limits. Procedural steps and all reported solution detection-limit values are transcribed with their limitations in Supplementary File S1, Section S20. The original samples are not currently available for new inductively coupled plasma mass spectrometry (ICP-MS) or X-ray fluorescence (XRF) measurements. The 32 historical rows are included without deletion; anomalous entries are flagged and subjected to sensitivity checks, not silently replaced. The declared source contains 1152 positive finite fraction entries and 288 reported four-fraction sums. Each reported sum agrees with the sum reconstructed from its four component fractions to rounding precision (maximum absolute difference 3.64×10^{-12} $\mu g\, g^{-1}$). This is a source-file completeness and arithmetic check, not a new check of FAAS analytical precision, detection-limit handling, or BCR fraction recovery. No flagged measurement is edited or omitted from the primary 32-row analysis (Supplementary File S1, Sections S19 and S20).

The thesis gives conflicting descriptions of the first sampling month. The discrepancy cannot be resolved at the record level and is not used analytically. Independent field-sampling design, site-replicate status, and magnetic calibration logs are not recoverable. Retrospective author clarification identifies the reported instrument family and nominal measurement frequencies, but cannot substitute for contemporaneous run-level calibration records. The historical measurements are reanalyzed here; no new sampling or laboratory measurements were performed.

2.2. Declared Analysis Source and Terminology

The declared analytical table has one row for each of 32 numbered historical soil records. For each of nine elements, it contains four operational fraction concentrations and their recorded four-fraction sum, giving 36 component-concentration fields and nine summed-concentration fields per record. Record-level metadata comprise the identifier, direction, factory-center distance in meters, latitude and longitude in degree–minute–second notation, low- and high-frequency susceptibility readings (LF and HF), specimen mass in grams, and the stored numerical mass-normalized magnetic fields XLF and XHF (whose physical scale is unresolved). Chemical fractions are paired attributes of the same record, not independent samples. The column mapping and source-file identifier are provided in Supplementary File S1, Section S1.

In retrospective clarification, the originating author identifies a Bartington Instruments MS2 Magnetic Susceptibility System, with nominal LF and HF frequencies of approximately 0.47 and 4.7 kHz. The literal LF/HF headers contain "Kvol", indicating a reported volumetric-susceptibility label rather than two separately applied magnetic fields; they do not certify the measurement scale. XLF and XHF denote the archived low- and high-frequency mass-normalized numerical fields, respectively, not independently calibrated SI mass-specific measurements. XLF is retained as the primary ranking variable because it is the available low-frequency mass-normalized numerical signal paired with all 32 chemical records. This provides one explicit ordering for the fixed-budget comparison without selecting a different primary magnetic variable after inspecting the chemical outcomes. The author reports nominally equal-volume holders but differing specimen masses; neither actual filled volumes nor the sensor head is independently documented. General MS2 documentation explains the importance of sample mass and measurement geometry [19]; it is not a calibration record for these specimens. Thus, the rationale for XLF does not establish physical comparability or validate the missing absolute scale. The analysis does not assume that XLF is universally superior to other magnetic properties. Available alternatives—XHF, raw LF and HF, and the LF/mass and HF/mass quotients—are assessed as ranking sensitivities; remanence, hysteresis, and mineral-specific magnetic measurements are not present in the admitted table.

The XLF/XHF columns have no independently verified International System of Units (SI) multiplier. The original MS2B instruction specifies a nominal 10 cm^3 measurement volume and 10-g mass normalization. If the historical LF readings are numerical volume susceptibilities in 10^{-5} SI, obtained with that MS2B geometry and applicable calibration, then the corresponding mass-specific susceptibility in $10^{-8}\,m^3\,kg^{-1}$ is $\chi_{LF}^{(10^{-8})} = 10\,LF/m_g$, where m_g is specimen mass in grams [19]. This is a factor of 10 relative to the direct LF/m_g numerical quotient used approximately in the archive; hence, archived XLF must not be labeled as a verified value in $10^{-8}\,m^3\,kg^{-1}$. For all 32 rows, LF/specimen mass differs from XLF by at most 0.04631 on the stored numerical scale; masses span 11.10–14.45 g. The agreement is consistent with rounded arithmetic normalization, not proof of instrument identity or calibration. A uniform positive factor of 10 applied to stored XLF cannot change the ranking or the primary retention comparisons, but a recalculation from unrounded LF/m_g need not preserve every tie. The conditional physical conversion and record-level differences are disclosed in Supplementary File S1, Section S19 and `MS2B_Conditional_Conversion_Audit.csv`; no stored value is replaced. The complete rank orders are not identical, but their eight selected record identifiers at $k = 8$ are identical. For HF/mass versus XHF, record 8 has an absolute discrepancy of 5.01477; the other 31 rows differ by at most 0.04944. The record-level arithmetic audit is provided in Supplementary File S1, Section S19 and the accompanying data table.

Percentage frequency-dependent susceptibility (XFD%) is calculated, not independently stored, as the secondary numerical diagnostic $100(XLF - XHF)/XLF$. At record 8, the stored XLF/XHF pair gives 26.5%, whereas the LF/HF pair gives approximately 1.26%. Its maximum falls from 26.5% to 6.19% when record 8, with inconsistent stored XHF, is omitted for sensitivity only. Supplementary File S1 also reports the corresponding raw-reading ratio. These checks do not establish a calibrated XFD-based screening rule. The field historically labeled "Total concentration (in all phases)" is numerically F1 + F2 + F3 + F4 and is called the four-fraction sum, not an independently measured total-digestion concentration. Although the thesis describes a separate strong-acid total digestion, a matched record-level total-digestion table is not available for this reanalysis.

No source value is silently corrected. Several discrepancies are retained as provenance flags. The five zero-distance workbook records are associated with the inside-factory label;

record 17 is not among them, and its coordinate lies approximately 563 m from the nearest zero-distance point. Its recorded distance of roughly 600 m is consistent with that spatial separation, whereas the thesis inside-group summary appears inconsistent. Record 1 Pb and record 11 Zn four-fraction sums are inconsistent with the corresponding thesis group maxima, but the available records do not establish a unique correction. Stored XHF at record 8 is inconsistent with the simple HF/specimen-mass calculation, whereas the eight-record XLF shortlist at $k = 8$ is unchanged by the alternative LF-based normalizations; the complete rank orders need not agree. These issues are handled by sensitivity analysis or explicit limitation. Supplementary File S1, Section S21 distinguishes the source table, thesis descriptions, retrospective author accounts, and current calculations, and provides a magnetic-field dictionary. Numerical consistency does not independently establish chemical accuracy, geometric comparability, or absolute calibration.

2.3. Historical Worksheet Crosswalk

The separate historical magnetic worksheet is an unpublished source document, used only for row-identity checks; the declared analytical table remains the numerical source. Its known identifier and verification limits are recorded in Supplementary File S1, Sections S10 and S21. It was compared row by row with the declared analytical table. Direction, latitude–longitude pairs, LF, HF, XLF, and XHF agree for all 32 records after trivial whitespace normalization. Historical numeric distances differ from the current positive distances by only 1–17 m in 15 of 27 rows; 12 of 27 are identical. Substituting the historical distances leaves the principal $k = 8$ Cu result unchanged. According to the originating author's retrospective explanation, codes 1–16 and 1n–16n were worksheet-organization labels rather than intended campaign or batch identifiers. No contemporaneous record-level field or laboratory ledger independently verifies this explanation. The recorded distance values also have visibly different precision conventions: records 1–16 use only round values (0, 200, 400, 600, 700, 800, and 1200 m), whereas records 17–32 include 150, 250, 260, 310, 360, 480, 770, 930, and 1150 m. This difference is observable in the archived table but does not independently establish separate collection campaigns or an explanation for the numerical half-split. The pronounced numerical differences between the halves may reflect undocumented collection or processing structure. The two row-order halves (1–16 and 17–32) are used only for sensitivity analysis; no causal or temporal interpretation is assigned.

2.4. Screening Rules and Chemical Targets

For a fixed budget k, magnetic selection ranks records by decreasing archived numerical XLF. Proximity selection ranks records by increasing recorded archival factory-center distance. Direction is retained for exploratory group-deletion sensitivity, but wind records are insufficient to construct a validated downwind-sector dispersion rule. When the cutoff contains ties, every admissible boundary choice is retained rather than resolved arbitrarily.

Three chemical targets are evaluated for each element: the four-fraction sum F1 + F2 + F3 + F4, F1 alone, and the combined non-residual sum F1 + F2 + F3. For a selected set S of k records and target value y_i for record i, retention is

$$R(S;k) = 100\,\frac{\sum_{i\in S} y_i}{\sum_{j=1}^{k} y_{(j)}}, \tag{1}$$

where $|S| = k$, $y_i > 0$, and $y_{(j)}$ denotes the jth-largest target among eligible records. Thus, $R(S;k)$ is dimensionless, belongs to $(0\%, 100\%]$, and equals 100% when the selected set captures the largest possible same-size target sum. The denominator is a retrospective chemical reference, not an implementable pre-analysis screening rule, because it requires the chemistry to be known.

A magnetic rule is classified as strictly better only when its worst admissible cutoff choice exceeds the best admissible proximity choice. The comparison is performed on the underlying 0–1 retention ratio before conversion to percent, using a numerical tolerance of 10^{-12}. Proximity is classified analogously; otherwise, the result is classified as overlap. The 10^{-12} tolerance in unitless ratio space is a deliberately conservative guard against binary floating-point differences that were observed below 10^{-14} in independent calculations; it is not an instrumental uncertainty, effect-size threshold or significance criterion. Calculations repeat $k = 1, \ldots, 31$ for all nine elements; at $k = 32$ both rankings select all 32 records and trivially retain 100%.

A complementary finite-record chance reference uses all equally probable $\binom{32}{8} = 10{,}518{,}300$ size-eight subsets. The exact expected percentage under uniform selection is $100(8/32)\sum_i y_i / \sum_{j=1}^{8} y_{(j)}$; the descriptive upper-tail p is the fraction of these subsets whose retention equals or exceeds the observed rule. A full enumeration is performed for each of 27 element–target outcomes, with tied proximity cutoffs reported as p ranges. These are conditional finite-record reference probabilities rather than independent-sample hypothesis tests; Cu was selected after examining nine elements, and multiplicity limits conventional interpretations of p.

Fixed-budget environmental sampling has long used inexpensive screening measurements to prioritize a smaller number of costly laboratory analyses [20]. The reusable decision logic here is: define the chemical target, rank candidate records with the inexpensive proxy, evaluate the selected set by target retention, compare against a simple field baseline, and repeat across budgets and sensitivity scenarios. Performance for one chemical target is not transferred automatically to another target from the same element. Secondary analyses reported in the Supplement use compositional-data reasoning for fraction shares [21,22] and a finite chemistry-informed observation-selection comparator [23]; these analyses are diagnostic and do not alter the primary two-rule comparison.

2.5. Sensitivity and Incremental-Value Analyses

The primary Cu comparison is evaluated by single-record deletion, pair deletion at $k = 8$, restriction to the 27 positive-distance records, the two agnostic row-order halves (each 16 records, evaluated at $k = 4$ and $k = 8$), omission of each recorded direction group, coordinate-derived separation, and the recovered historical distance column. The half-split is not interpreted as a campaign comparison. Alternative magnetic rankings use stored XHF, raw LF and HF, and the LF/mass and HF/mass quotients. The coordinate-derived comparison is an internal sensitivity check and does not establish a factory boundary or emission origin.

Because the thesis inside-group summary conflicts with record 17's workbook distance, an additional stress-test sets record 17's distance to zero without changing any chemistry or magnetic value. Coordinates favor the original approximately 600-m assignment; the zero-distance counterfactual remains in Supplementary File S1 as a robustness test, not an equally plausible field correction.

A deliberately small exploratory model tests whether XLF contains information beyond recorded distance. Both model specifications use ordinary least squares (OLS). Standard errors (SE) are model-based, and R^2 denotes the coefficient of determination. Let $Y > 0$ denote the Cu chemical target for a record, $d \geq 0$ its recorded distance, and $x > 0$ its stored XLF value. To make the logarithms dimensionless without changing the numerical fits, define reference values $Y_0 = 1\ \mu g\, g^{-1}$, $d_0 = 1$ m, and $x_0 = 1$ unit of the stored numerical XLF scale. Let α_0 and α_1 denote the intercept and distance coefficient in the distance-only

model, and let β_0, β_1, and β_2 denote the coefficients in the distance-plus-XLF model. The distance-only model is

$$\ln(Y/Y_0) = \alpha_0 + \alpha_1 \ln(1 + d/d_0), \quad (2)$$

and is compared with

$$\ln(Y/Y_0) = \beta_0 + \beta_1 \ln(1 + d/d_0) + \beta_2 \ln(x/x_0). \quad (3)$$

The operator ln denotes the natural logarithm. Performance is assessed by leave-one-out root-mean-square error (RMSE) on the log scale. No variable selection, interaction search, machine learning, or separate hold-out train/test partition is used.

2.6. Statistical Interpretation and Reproducibility

The primary outputs are finite-record decision comparisons, not estimates of a superpopulation treatment effect. Retention percentages therefore describe how much of an observed chemical target is captured by a screening rule within the declared candidate table. Main-text retention percentages are displayed to one decimal place to avoid implying unsupported analytical precision; all ranking, tie and chance-reference calculations use unrounded values, retained in the supplementary electronic tables. Tie ranges are propagated explicitly, and sensitivity analyses are reported as changes in decision classification rather than converted into nominal significance tests. Cu was selected after inspection of the full nine-element comparison and is therefore exploratory rather than confirmatory.

The baseline repository records an earlier Windows-based computational environment. The accompanying revision analyses and verifier were executed using Python 3.13.5, NumPy 2.3.5, and SciPy 1.17.0 on Linux. The environment record and portable commands are included with Supplementary Data. During preparation, OpenAI ChatGPT and OpenAI Codex assisted with literature searches, analysis planning, code development and checks, and manuscript drafting and editing. All reported numerical outputs were calculated from the archived workbook using executable scripts and evaluated through the reproduction checks described here and in Supplementary Data; the tools did not provide or modify any field or laboratory measurements. The disclosure of AI assistance is given in Acknowledgments. The graphical abstract was generated reproducibly in Python from the audited $k = 8$ Cu retention table; its distance-selection ranges denote admissible tie choices, not confidence intervals or new field measurements. The plotting code is included with Supplementary Data. The original analytical table and the scientific values of its metadata-sanitized derivative remain unchanged. New verification covers the 837 ordinary element–target–budget cases, the printed $k = 8$ retentions, and the chance-reference, correlation, regression, coordinate, and record-order calculations. Historical deletion, crosswalk, and secondary minimum-of-four diagnostics remain separately documented in the baseline repository.

A public November 2026 code snapshot provides a single-command replay from the unchanged metadata-sanitized source workbook. The clean-extraction audit checks the 837 element–target–budget calculations and reproduces all four manuscript/supplement figures; in the documented environment the reproduced PDF figure pages have identical dimensions and pixels to the fixed source figures at 216 dpi. These checks verify arithmetic and rendering, not the original instrument calibration, chemical recovery, or predictive performance at new sites.

3. Results

3.1. All-Element Target Dependence

Across the 31 possible selection budgets, the balance between magnetic and proximity selection varied by both element and chemical target. The strongest consistent magnetic

preference occurred for Mn: magnetic selection was strictly better at 28 of 31 budgets for both the four-fraction and non-residual sums. Cu showed the clearest target reversal. For the four-fraction Cu sum, magnetic selection was strictly better at 24 budgets, proximity at 3, and 4 overlapped. For non-residual Cu, the pattern reversed: magnetic selection was better at only 2 budgets, proximity at 24, and 5 overlapped. F1 Cu was intermediate, with 14 magnetic, 12 proximity, and 5 overlap classifications. Table 1 summarizes these counts.

Table 1. Strict winner counts across $k = 1$–31 (M: strict XLF advantage; P: strict proximity advantage; O: overlap); each cell sums to 31. XLF is the archived mass-normalized low-frequency magnetic index; F1 is the acid-soluble first fraction; non-residual denotes F1 + F2 + F3. Cd and Cr have unresolved numerical-provenance flags; pairwise winners do not imply above-chance recovery.

Element	Four-Fraction Sum	F1	Non-Residual
Cd	21/2/8	25/0/6	19/4/8
Co	13/13/5	10/17/4	11/15/5
Cr	13/9/9	21/5/5	12/8/11
Cu	24/3/4	14/12/5	2/24/5
Fe	13/12/6	17/9/5	13/9/9
Mn	28/0/3	25/3/3	28/0/3
Ni	20/6/5	17/7/7	14/9/8
Pb	16/13/2	16/12/3	16/13/2
Zn	15/11/5	10/11/10	14/10/7

At $k = 8$, magnetic selection is strictly better for all three Mn targets. Proximity is strictly better for all three Co, Fe, and Pb targets in the complete 32-record set, but the ordering for Co and Fe is sensitive to candidate-set definition (Section 3.6). Cu is the only element at this budget with the specific magnetic/magnetic/proximity pattern across four-fraction sum, F1, and non-residual sum. Figure 2 summarizes the target-aware classification across all elements, targets, and budgets.

3.2. Descriptive Fraction Concentrations in the Historical Table

To make the operational fraction differences transparent, Table 2 reports the median of each recorded fraction across all 32 rows. F4 is frequently prominent in the recorded Cu values, but these medians are not an independently measured total concentration or an environmental contamination index. Medians of separately recorded fractions need not sum to the median of their four-fraction total. Cd and Cr contain unresolved numerical patterns; Pb and Zn have specific unresolved source-magnitude flags, so this table is descriptive rather than new chemical validation.

3.3. Cu Reversal at a Quarter-Size Budget

The eight records with the highest XLF values are records 8, 12, 16, 19, 24, 26, 29, and 31. Using Equation (1), these records retain 91.7% of the best achievable four-fraction Cu sum and 84.3% of the best achievable F1 Cu sum at $k = 8$. The six admissible nearest-distance selections retain 84.7–87.6% and 74.1–77.3%, respectively. XLF selection therefore strictly exceeds the distance rule for these two targets. The four-fraction Cu XLF result has a small unadjusted finite-subset upper-tail fraction ($p = 0.017$), but Cu was selected post hoc and this comparison is not a population-level significance test.

Table 2. Median recorded concentration ($\mu g\,g^{-1}$) of each operational fraction across 32 historical rows. Each column is summarized separately; displayed precision is descriptive, not instrumental accuracy. F4 represents the thesis's additional residual microwave digestion. Cd and Cr retain unresolved numerical-pattern flags; no entry is excluded or corrected.

Element	F1 Acid Soluble	F2 Reducible	F3 Oxidizable	F4 Residual
Cd	0.078	0.098	0.026	0.093
Co	14.1	24.9	8.44	30.1
Cr	0.182	0.168	2.58	31.4
Cu	2.63	3.74	1.79	23.0
Fe	28.0	728	295	10,424
Mn	66.6	754	112	207
Ni	10.4	18.7	15.0	39.8
Pb	71.6	45.1	28.3	91.2
Zn	9.69	51.7	21.4	108

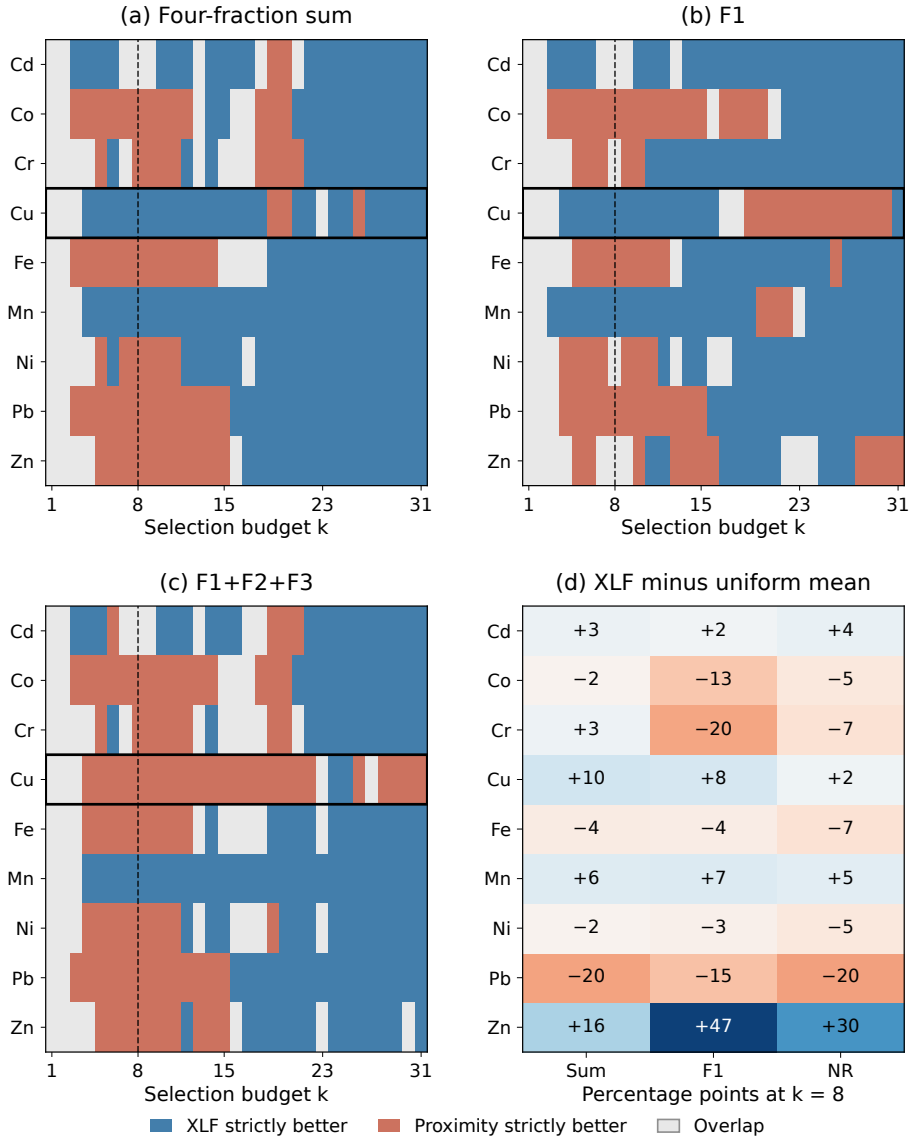


Figure 2. Panels (**a**–**c**): winners across four-fraction, F1 and non-residual targets (blue: XLF; terracotta: proximity; gray: overlap). Panel (**d**): XLF minus uniform-subset mean at $k = 8$ (percentage points; blue: positive, terracotta: negative; darker color: larger magnitude). NR denotes non-residual (F1 + F2 + F3). Not a significance test. Dashed lines mark $k = 8$; Cu outlined. Cd/Cr have provenance flags.

For the non-residual Cu sum, the ordering reverses. The magnetic set retains 60.3%, whereas the admissible proximity sets retain 80.8–86.6%. Thus, an XLF-based shortlist that retains a large share of the four-fraction Cu sum does not recover the records with the largest combined F1 + F2 + F3 Cu concentrations. Table 3 places this reversal within the complete all-element comparison, and Figure 3 shows how the Cu comparison changes across budgets.

Table 3. Retention at $k = 8$ for all nine elements. Values: XLF retention/admissible distance-selection range (%). M denotes strict XLF winner over proximity, P strict proximity winner, and O overlap. Displayed retentions are rounded to one decimal place; all winner classifications use the unrounded source values, not displayed precision; Cd and Cr have unresolved numerical-pattern provenance flags.

Element	Four-Fraction Sum	F1	Non-Residual
Cd	35.1/31.3–50.0 (O)	35.2/29.7–51.0 (O)	36.2/32.9–53.0 (O)
Co	66.8/82.2–86.1 (P)	51.3/74.8–80.9 (P)	60.3/81.6–87.2 (P)
Cr	49.7/54.3–59.1 (P)	7.3/5.4–36.3 (O)	27.5/31.0–43.5 (P)
Cu	91.7/84.7–87.6 (M)	84.3/74.1–77.3 (M)	60.3/80.8–86.6 (P)
Fe	66.5/86.2–90.5 (P)	57.3/64.1–73.3 (P)	27.6/45.6–65.7 (P)
Mn	76.5/57.0–62.7 (M)	72.0/50.6–54.5 (M)	73.1/52.8–59.1 (M)
Ni	71.2/77.0–79.9 (P)	63.4/63.1–72.5 (O)	63.1/73.4–79.6 (P)
Pb	14.4/25.7–27.3 (P)	29.2/46.9–52.4 (P)	12.3/21.6–23.0 (P)
Zn	60.4/64.3–94.7 (P)	77.6/76.1–86.5 (O)	69.0/72.8–95.6 (P)

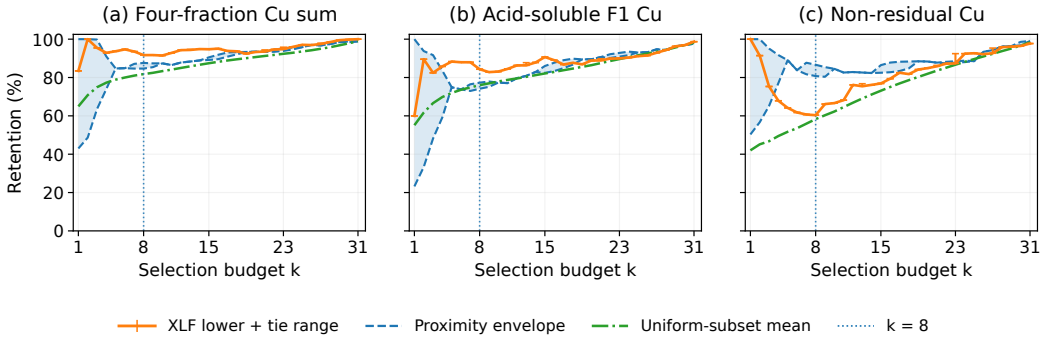


Figure 3. Cu retention by selection budget: (**a**) four-fraction Cu sum; (**b**) acid-soluble F1 Cu; and (**c**) non-residual Cu. The solid curve is the lower XLF cutoff envelope; vertical bars show the full XLF range where a tied cutoff permits different selections. The shaded region and dashed curves show the proximity envelope. The dot-dashed curve is the exact uniform-subset expectation; the vertical dotted line marks $k = 8$. Both envelopes describe cutoff-choice ambiguity, not statistical confidence intervals. Common x-axis ticks are used for all three targets.

Table 4 summarizes the three Cu chance-reference comparisons.

Table 4. Exact finite-record chance context at $k = 8$. The p values are one-sided uniform-subset upper-tail fractions over $\binom{32}{8}$ size-eight sets, not inferential claims over a sampled population; Cu was chosen post hoc.

Cu Target	XLF (%)	Random Mean (%)	XLF p	Proximity p Range
Four-fraction sum	91.7	81.8	0.017	0.109–0.267
F1	84.3	76.0	0.099	0.409–0.606
Non-residual	60.3	58.3	0.392	0.0009–0.0071

All 27 element–target chance comparisons are reproducible from the supplementary CSV; for example, Mn four-fraction XLF retention is 76.5%, but its upper-tail chance-reference

$p = 0.207$. Pb may be proximity-favored relative to XLF despite failing to exceed the uniform reference. Thus, a strict pairwise winner does not, by itself, establish universal proxy validity.

3.4. Cu Fraction-Level Magnetic Association

The within-record Cu F4 share of the four-fraction sum has a mean of approximately 67% and a median of 74.5%. This operational fraction does not identify the minerals responsible for the magnetic signal. Spearman rank correlations of XLF with Cu are $\rho = 0.437$ for the four-fraction sum ($p = 0.012$) and $\rho = 0.106$ for the non-residual sum ($p = 0.565$), consistent with the decision-level target reversal. Individual fractions show limited evidence for a simple phase-specific mechanism (Table 5). These nominal correlation p values are descriptive, not corrections for endpoint multiplicity.

Table 5. Spearman correlation between recorded XLF and each Cu fraction (32 records).

Cu Endpoint	Spearman ρ	Nominal Two-Sided p
F1	0.174	0.340
F2	0.127	0.488
F3	−0.011	0.953
F4	0.296	0.100
Four-fraction sum	0.437	0.012
Non-residual (F1 + F2 + F3)	0.106	0.565

3.5. Record Influence and Candidate Scope

All 32 single-record omissions retain the three-target $k = 8$ Cu pattern. Pair deletion retains the full three-target pattern for 490 of 496 omitted pairs, and the simpler four-fraction/non-residual reversal survives 494 of 496 pairs. Proximity retains the non-residual advantage after all 496 pair deletions. All six compared magnetic representations (XLF, XHF, raw LF, raw HF, LF/mass and HF/mass) select the same eight records at $k = 8$; this is a ranking stability result, not an independent calibration check. The reversal is nevertheless conditional on the eligible population and selected fraction: restricting the analysis to positive-distance records weakens the F1 component, but both record-order halves retain the M/M/P Cu pattern at $k = 8$ within each half. At the within-half quarter-budget $k = 4$, the pattern is M/O/O in rows 1–16 and M/M/M in rows 17–32. The record-order halves cannot be assigned to separate field sampling campaigns or laboratory batches without a contemporaneous record-level ledger. These findings support a finite-record screening interpretation rather than a claim of population-level transportability.

3.6. Sensitivity of Co, Fe and Pb to Candidate-Set Definition

The strong nearest-distance preference for Co, Fe and Pb in the complete 32-row table at $k = 8$ is not uniformly transportable to order-defined subsets. Table 6 compares the same fixed count $k = 8$ within each half; that count represents 50% rather than 25% of the eligible half. For Co and Fe, at least one chemical target changes winner or becomes overlapping; Pb remains distance-favored for all three targets in both halves. Cu retains its original M/M/P classification at $k = 8$ in each half, although the more comparable within-half quarter-budget $k = 4$ results differ. Full retention envelopes, $k = 4$ classifications, and candidate counts are reported in the "Extended record-order contrasts for Co, Fe, Pb and Cu" section of Supplementary File S1 and the machine-readable 60-comparison audit. These groups are defined solely by archival row order; they are not verified sampling campaigns, spatial holdouts, or independent external test sets.

Table 6. Fixed-count $k = 8$ winner classification for four contrasted elements and three chemical targets (sum/F1/non-residual). M: strict XLF advantage; P: strict nearest-distance advantage; O: cutoff-envelope overlap. Each row-half contains $n = 16$; the complete set contains $n = 32$.

Eligible Candidates	Co	Fe	Pb	Cu
All 32 records	P/P/P	P/P/P	P/P/P	M/M/P
Records 1–16	M/O/M	M/M/O	P/P/P	M/M/P
Records 17–32	P/M/M	M/M/P	P/P/P	M/M/P

3.7. Coordinate Evidence and Counterfactual Record-17 Sensitivity

Recorded coordinates place record 17 approximately 563 m from its closest zero-distance point, supporting the declared approximately 600-m entry rather than the thesis inside-group summary. To be conservative, setting only record 17's distance to zero as a counterfactual still does not change the $k = 8$ target ordering. Under this scenario, proximity retention is 86.5–88.6% for the four-fraction Cu sum, 73.7–76.8% for F1, and 79.6–85.0% for the non-residual sum. Magnetic retention remains 91.7%, 84.3%, and 60.3%, respectively.

3.8. Does XLF Add Information Beyond Distance?

For the four-fraction Cu sum, adding the XLF term in Equation (3) to the distance-only model in Equation (2) reduces log-scale leave-one-out RMSE from 0.2099 to 0.1655, an improvement of 21.1%. For F1 Cu, the reduction is only 1.5% (0.3174 to 0.3128). For non-residual Cu, adding XLF increases RMSE by 6.5% (0.3492 to 0.3718). Table 7 summarizes these exploratory diagnostics.

Table 7. Leave-one-out log-scale RMSE for Cu models. Positive change denotes improvement after adding XLF.

Cu Target	Distance Only	Distance + XLF	Change
Four-fraction sum	0.2099	0.1655	+21.1%
F1	0.3174	0.3128	+1.5%
Non-residual	0.3492	0.3718	−6.5%

Table 8 reports the descriptive coefficients and standard errors for the two-predictor fits.

Table 8. Descriptive OLS estimates for the distance + XLF model in Equation (3). All coefficients and standard errors are on the natural-log response scale, with $n = 32$; nominal p values exclude model-selection uncertainty.

Cu Target	Term	Estimate	SE	p	R^2
Four-fraction sum	Intercept	2.508	0.229	<0.001	0.431
	$\ln(1 + d/d_0)$	+0.021	0.013	0.123	
	$\ln(\mathrm{XLF}/x_0)$	+0.373	0.081	<0.001	
F1	Intercept	0.199	0.435	0.651	0.089
	$\ln(1 + d/d_0)$	+0.028	0.025	0.281	
	$\ln(\mathrm{XLF}/x_0)$	+0.256	0.154	0.108	
Non-residual	Intercept	3.038	0.541	<0.001	0.375
	$\ln(1 + d/d_0)$	−0.117	0.031	0.0008	
	$\ln(\mathrm{XLF}/x_0)$	−0.074	0.192	0.704	

Full coefficients for both specifications are supplied in the electronic coefficient table (Cu_OLS_coefficients.csv). Supplementary File S1, Section S22 tabulates the distance-only estimates, standard errors and nominal tests. For four-fraction Cu, the distance-only R^2 is just 0.017, compared with 0.431 when XLF enters. The distance coefficient in the two-variable fit is slightly positive and imprecise, so the apparent RMSE improvement mainly

reflects XLF information rather than a monotonic concentration decline with distance. For non-residual Cu, the pattern reverses: the distance-only R^2 is 0.372; in the two-predictor fit, the distance coefficient is −0.117 (SE 0.031; nominal $p = 0.0008$), while XLF is not associated with an additional detectable contribution (nominal $p = 0.704$). These are complementary diagnostics on the same 32 archival records, not an independent validation experiment. XLF and distance are themselves correlated (Spearman −0.55), complicating coefficient interpretation. The leave-one-out errors are point estimates from 32 historical records and have not been externally validated.

The same qualitative model tendency persists when record 17 is assigned zero distance: the two-predictor model improves four-fraction-sum RMSE by 16.3%, changes F1 RMSE by only 1.6%, and worsens non-residual RMSE by 6.9%. These models are not proposed as calibrated predictors; they provide a compact diagnostic consistent with the selection analysis.

4. Discussion

4.1. Screening Performance Depends on the Chemical Target

The central descriptive result is a reversal in fixed-budget decision performance that is consistent with a change in correlation structure between XLF and Cu fractions; neither result is proof of a physical carrier phase. At the same selection budget, using the same candidate records and the same magnetic ranking, the preferred screening rule changes when the Cu target changes. XLF exceeds the distance rule for the four-fraction sum and F1 at $k = 8$, but F1 does not clearly exceed uniform chance ($p = 0.099$). For the combined non-residual pool, XLF performs near the chance mean ($p = 0.392$), while distance gives lower nominal uniform-subset upper-tail fractions (0.0009–0.0071). A statement that magnetic susceptibility "screens Cu well" is therefore incomplete unless the chemical target is specified.

This distinction matters for monitoring design because magnetic and sequential-extraction measurements encode different properties. XLF reflects magnetic characteristics of the sampled material, whereas BCR fractions reflect operational extractability under defined chemical steps. Their association can therefore be target-specific rather than interchangeable. The relevant question is not only whether two variables correlate, but whether a proxy prioritizes the records that matter for the stated chemical objective.

4.2. Relation to Previous Magnetic and Fractionation Studies

Previous industrial-soil and sediment studies show that magnetic susceptibility can identify metal-enriched locations, but they also emphasize site-specific control. Cao et al. [12] moved beyond correlation by showing that magnetic pre-screening can improve targeted chemical site assessment. Wang et al. [7] demonstrated that susceptibility–metal relationships can differ among sequentially extracted fractions, while Ye et al. [13] developed additional magnetic proxies associated with source and operational availability. The present study occupies a different niche: it holds the proxy and candidate records fixed and asks whether the preferred screening rule changes solely because the chemical target changes.

Recent estuarine work [24] presented magnetic susceptibility as a rapid screening proxy while emphasizing local calibration and chemical validation. A 2026 *Environments* study around an iron-ore complex likewise showed that total and operationally mobile metal pools can lead to different environmental interpretations [25]. The finite-record results extend this distinction to screening decisions: successful recovery of a summed concentration does not establish successful recovery of an operationally non-residual target.

The broader literature supports both sides of this interpretation. Magnetic susceptibility has been used to map or screen pollution in roadside, urban, and industrial soils across

multiple settings [26–30], while sequential-extraction studies emphasize that extracted pools are operationally defined and procedure-dependent rather than direct measurements of unique mineral phases or realized availability [15,31].

ISO 21226:2019 describes soil magnetometry as a screening method for identifying areas that may require follow-up geochemical investigation [32]. However, elevated magnetic susceptibility alone does not establish which individual samples should be prioritized for every operational chemical fraction of a metal. The standard addresses screening for potential trace-element pollution associated with technogenic magnetic particles; it does not validate fraction-specific sample rankings for this historical cohort.

The present results suggest a practical way to examine this distinction. Before applying a magnetic proxy to select samples for chemical analysis, the operational chemical target and the affordable number of assays should be specified. The magnetic ranking can then be compared with a clearly defined alternative, allowing for cutoff ties and a same-budget uniform-random reference. In these records, the same XLF ranking outperforms proximity for the four-fraction Cu sum at $k = 8$, but underperforms proximity for non-residual Cu. Its apparent advantage for F1 Cu also does not clearly exceed the uniform-random reference ($p = 0.099$).

Thus, favorable screening performance for one chemical target cannot be transferred automatically to another, even for the same element and sampled locations. The fixed-budget, target-conditioned comparison is reproducible for the archived data, but neither rule has been prospectively validated at other sites.

4.3. Proximity and Magnetism Provide Different Information

The comparison with distance from the factory center is intentionally simple. Distance is not a complete transport model and does not encode wind, topography, soil properties, or source heterogeneity. Nevertheless, it represents a plausible low-information field rule against which a magnetic ranking can be evaluated. The incremental model check is consistent with the decision comparison: adding XLF reduces leave-one-out error for the four-fraction Cu sum relative to a weak distance-only model, whereas it does not improve the non-residual target. These results concern this distance-only rule, not all spatial screening strategies. A direction- or wind-informed rule could perform differently, but no validated historical downwind weighting is available in these records.

4.4. Recovered Provenance Strengthens, but Does Not Erase, Historical Limitations

Recovery of the factory thesis substantially improves analytical provenance: sampling depth, BCR-based extraction and the subsequent modified F4 digestion, FAAS measurement, and historical QA/QC procedures are documented, while the historical magnetic worksheet provides a row-identity cross-check. This documentation must not be confused with demonstration of uniformly accurate chemistry. SRM Table 2.3 of the 2015 thesis contains a conspicuous Cd discrepancy (420% as a measured/reference ratio), incomplete reference entries and an inconsistent first-SRM identifier. The SRMs are described as microwave-digested; they do not independently establish the recovery of individual BCR fractions. No use of BCR-701 or an equivalent fraction-specific sequential-extraction CRM is documented in the available sources. The nine reported detection limits are solution concentrations in mg/L, not independently traced thresholds for each fraction in the 32-record soil workbook. No row-level censoring/substitution ledger, independent total-digestion worksheet, or fraction-level recovery record is available (Supplementary File S1, Section S20).

Record inclusion and arithmetic reproducibility, source-level QA/QC reporting, and independent chemical validity are distinct evidentiary claims. The present calculations establish transformations and rule comparisons conditional on the archived measurements;

they do not establish unbiased assays or validated fraction recovery. These recovered sources do not justify silent reconstruction of uncertain values. The discrepancy in the thesis summary for record 17, the magnitude differences for record 1 Pb and record 11 Zn, repeated Cr fraction ratios, repeated Cd four-fraction sums, and the record 8 XHF inconsistency remain provenance flags. The author associates some low Cd/Cr values with detection limitations, but the available sources do not document an exact substitution/censoring rule, so Cd and Cr results are reported descriptively without claiming verified fraction-specific recovery. These flagged entries are not inputs to the Cu target values or the primary stored-XLF ordering; this separation does not independently validate Cu chemistry. Hypothetical Pb/Zn correction scenarios are retained only in the Supplementary Materials and do not modify the declared workbook.

The magnetic-unit correction also distinguishes ranking stability from physical measurement validity. Multiplying every stored XLF value by the same positive conversion factor preserves its ordering, its ties, and the corresponding ranking-based screening comparisons. This mathematical invariance does not verify the archived sensor-head configuration, filled specimen volume, or run-specific calibration. A stable selection decision should therefore not be presented as independent confirmation of the physical susceptibility scale.

4.5. Limitations

This secondary analysis uses 32 historical soil records from one industrial setting. The thesis contains a historical sampling image, but an independently verified georeferenced site map, surveyed factory boundary, and local background comparator are unavailable. Figure 1 provides a locator and coordinate reconstruction, not a field survey. The absence of a matched local background and independently validated site conditions prevents a defensible enrichment or regulatory-exceedance classification; thresholds for unrelated sites or different chemical pools are therefore not applied. Cu was selected after inspection of the complete nine-element comparison and is therefore exploratory rather than a pre-registered hypothesis. The original thesis documents the BCR-based chemical extraction sequence, including its modified residual digestion, and retrospective author testimony reports the Bartington MS2 instrument family and nominal measurement frequencies, but this evidence does not establish the original sampling design, independence among records, or run-specific calibration. The three BCR extraction fractions and the subsequent residual-digestion fraction are operationally defined analytical pools and should not be interpreted as exact mineral species, realized environmental release, bioaccessibility, or health risk [17,18]. The historical SRM table reports variable agreement with listed reference values and has unresolved identifier/units metadata; it cannot support a blanket claim of analytical recovery. The study has no contemporary resampling, uncontaminated local background, independent external validation set, or measurements of soil pH, organic matter, texture, mineralogy, or source tracers. The results therefore establish what follows from the recovered records; they do not validate a universal magnetic threshold or a transferable prediction model.

5. Conclusions

Magnetic screening performance in this dataset depended on the chemical target used to judge the rule. At $k = 8$, XLF exceeded the proximity rule for the four-fraction Cu sum and F1 Cu but underperformed for non-residual Cu. For four-fraction Cu, the unadjusted finite-subset upper-tail fraction was 0.017; this does not establish a multiplicity-adjusted population-level result. At $k = 8$, the three-target pattern survived all 32 single-record deletions and 490 of 496 pair deletions, but not every candidate-set or budget change. Across the nine elements, neither screening rule was universally superior.

The broader implication is methodological: a rapid environmental proxy should be validated against the chemical endpoint it is intended to prioritize. The exploratory leave-one-out comparison broadly tracked the decision result, but was not a calibrated predictive validation: adding XLF improved prediction beyond distance for the four-fraction Cu sum but not for non-residual Cu. Evidence that a magnetic measure identifies records with high summed concentrations cannot be transferred automatically to operationally defined fractions of the same element. These findings are specific to the recovered historical dataset and do not establish a universal magnetic threshold or transferable field model. Prospective monitoring studies should therefore define the chemical target before selecting or validating a screening proxy.

Future Work: Independent Validation

Assessing transfer requires field replication with a prospectively documented sampling frame, verified specimen volume and mass normalization, fraction-specific recovery references, local background samples, and spatially resolved wind observations. Such evidence would test whether the target-dependent screening result persists beyond these historical records.

Supplementary Materials: The following supporting information can be downloaded at: https://www.mdpi.com/article/10.3390/environments13110627/s1, Supplementary File S1: Supplementary methods and results. Additional details include the element-by-target classifications across $k = 1$–31, tie handling, single- and pair-deletion analyses, candidate-scope and coordinate-derived-distance checks, the historical worksheet crosswalk, reproducibility diagnostics, the record-17 zero-distance sensitivity, leave-one-out model predictions, and clearly labeled hypothetical Pb/Zn provenance-sensitivity scenarios. The accompanying Supplementary Data supplies the primary classification grid, supporting numerical tables, a conditional MS2B unit-conversion audit, and a transcription-derived audit of the original thesis QA/QC table and detection limits. Historical tie selections, deletion results, crosswalks, and secondary diagnostics are retained in the baseline repository identified in the Data Availability Statement. These scenarios do not replace or modify the declared analysis workbook.

Author Contributions: Data curation, investigation, and writing—review and editing, I.F.A.-M.; conceptualization, methodology, and writing—review and editing, M.S.L.; investigation, sample collection, original experimental work, thesis data curation, and writing—review and editing, E.K.A.-S.; writing—original draft preparation and writing—review and editing, G.M.; software, formal analysis, and writing—review and editing, A.E.; supervision, project administration, and writing—review and editing, H.A. All authors have read and agreed to the published version of the manuscript.

Funding: The research project that provided the data for this reanalysis was financially supported by the Scientific Research and Innovation Support Fund (SRISF), Jordan. The authors gratefully acknowledge this support. The article processing charges (APCs) are supported by Higher Colleges of Technology (HCT).

Institutional Review Board Statement: Not applicable. This secondary analysis used non-human environmental data and involved no human participants or animals.

Informed Consent Statement: Not applicable.

Data Availability Statement: The materials approved for public release for this secondary analysis are available through one public GitHub repository: https://github.com/shaikhamalkawi-ux/iron-factory-copper-screening (accessed on 8 November 2026). These include the unchanged metadata-sanitized 32-record workbook (`source/Iron Factory.xlsx`), the executable November 2026 numerical and four-figure replay packages (`nov2026_revision/`), derived results and integrity checks, and the unmodified 2015 Yarmouk University MSc thesis by Al-Sharadqah (`thesis/Al-Sharadqah_2015_Yarmouk_MSc_Thesis.pdf`). The repository README provides the file organization, reproduction instructions, and source checksums. The historical thesis is a reading copy with its own rights notice, not an extension of the repository's code or data licences. The unredacted origi-

nal workbook is not publicly redistributed. Supplementary Data S2 also provides revision-specific calculations. The earlier Zenodo dataset/software DOI refers to a separate older deposit, not the November 2026 source release. Source-to-output reproduction does not independently establish calibration, fraction-level chemical recovery, or external field generalizability.

Acknowledgments: During the preparation of this manuscript, the authors used OpenAI ChatGPT-6 and OpenAI Codex for literature-search assistance, manuscript drafting and editing, and development and checking of analysis code. The accompanying graphical abstract was rendered from the audited numerical table using the supplied Python plotting script; it does not represent any new field or laboratory observation. The available project records do not reliably identify every model or software-build version used during this extended workflow, so a specific historical version is not asserted. The authors reviewed and edited the outputs and take full responsibility for the content of this publication. All empirical measurements came from the recovered source materials and were not generated or altered by artificial intelligence.

Conflicts of Interest: The authors declare no conflict of interest.

References

1. Schmidt, A.; Yarnold, R.; Hill, M.; Ashmore, M. Magnetic susceptibility as proxy for heavy metal pollution: A site study. *J. Geochem. Explor.* **2005**, *85*, 109–117. [CrossRef]
2. Blaha, U.; Appel, E.; Stanjek, H. Determination of anthropogenic boundary depth in industrially polluted soil and semi-quantification of heavy metal loads using magnetic susceptibility. *Environ. Pollut.* **2008**, *156*, 278–289. [CrossRef] [PubMed]
3. Lu, S.; Wang, H.; Bai, S. Heavy metal contents and magnetic susceptibility of soils along an urban–rural gradient in rapidly growing city of Eastern China. *Environ. Monit. Assess.* **2009**, *155*, 91–101. [CrossRef] [PubMed]
4. Rachwał, M.; Magiera, T.; Wawer, M. Coke industry and steel metallurgy as the source of soil contamination by technogenic magnetic particles, heavy metals and polycyclic aromatic hydrocarbons. *Chemosphere* **2015**, *138*, 863–873. [CrossRef] [PubMed]
5. Magiera, T.; Zawadzki, J.; Szuszkiewicz, M.; Fabijańczyk, P.; Steinnes, E.; Fabian, K.; Miszczak, E. Impact of an iron mine and a nickel smelter at the Norwegian/Russian border close to the Barents Sea on surface soil magnetic susceptibility and content of potentially toxic elements. *Chemosphere* **2018**, *195*, 48–62. [CrossRef] [PubMed]
6. Zhao, X.; Zhang, J.; Ma, R.; Luo, H.; Wan, T.; Yu, D.; Hong, Y. Worldwide Examination of Magnetic Responses to Heavy Metal Pollution in Agricultural Soils. *Agriculture* **2024**, *14*, 702. [CrossRef]
7. Wang, C.; Ma, R.; Wang, J.; Zhong, C.; Zhao, Y.; Browne, P. Fractionations of heavy metals and their correlations with magnetic susceptibility in soil from a typical alluvial island in the lower Yangtze River, China. *J. Clean. Prod.* **2023**, *418*, 138060. [CrossRef]
8. Al-Sharadqah, E.K. Sequential Fractionation of Heavy Metals in Soils Around the Iron Smelting Factory in Mafraq, Jordan. Master's Thesis, Yarmouk University, Irbid, Jordan, 2015.
9. Yang, P.; Drohan, P.J.; Yang, M. Patterns in soil contamination across an abandoned steel and iron plant: Proximity to source and seasonal wind direction as drivers. *CATENA* **2020**, *190*, 104537. [CrossRef]
10. Rachwał, M.; Wawer, M.; Magiera, T.; Steinnes, E. Integration of soil magnetometry and geochemistry for assessment of human health risk from metallurgical slag dumps. *Environ. Sci. Pollut. Res.* **2017**, *24*, 26410–26423. [CrossRef] [PubMed]
11. Jabłońska-Czapla, M.; Rachwał, M.; Grygoyć, K.; Wawer-Liszka, M. Application of soil magnetometry and geochemical methods to investigate soil contamination with antimony. *Environ. Geochem. Health* **2024**, *46*, 287. [CrossRef] [PubMed]
12. Cao, L.; Appel, E.; Rösler, W.; Magiera, T. Efficiency of stepwise magnetic-chemical site assessment for fly ash derived heavy metal pollution. *Geophys. J. Int.* **2015**, *203*, 767–775. [CrossRef]
13. Ye, J.; Wu, J.; Shi, T.; Chen, C.; Li, J.; Wang, P.; Song, Y.; Yu, Q.; Zhu, Z. New magnetic proxies to reveal source and bioavailability of heavy metals in contaminated soils. *J. Hazard. Mater.* **2024**, *479*, 135665. [CrossRef] [PubMed]
14. Natural Earth. 1:110m Cultural Vectors: Admin 0 Countries. Generalized National Outline Used Only for the Study-Area Locator; Local Boundary Geometry Is Archived with the Figure Source. Available online: https://www.naturalearthdata.com/downloads/110m-cultural-vectors/110m-admin-0-countries/ (accessed on 25 October 2026).
15. Rauret, G.; López-Sánchez, J.F.; Sahuquillo, A.; Rubio, R.; Davidson, C.; Ure, A.; Quevauviller, P. Improvement of the BCR three step sequential extraction procedure prior to the certification of new sediment and soil reference materials. *J. Environ. Monit.* **1999**, *1*, 57–61. [CrossRef] [PubMed]
16. European Commission, Joint Research Centre. *The Certification of the Extractable Contents (Mass Fractions) of Cd, Cr, Cu, Ni, Pb and Zn in Freshwater Sediment Following a Sequential Extraction Procedure (BCR-701)*; Technical Report EUR 19775 EN; European Commission: Luxembourg, 2001; Annex II, pp. 71–73. Available online: https://crm.jrc.ec.europa.eu/sites/default/files/afas/BCR-701_report_2.pdf (accessed on 25 October 2026).

17. Quevauviller, P. Operationally defined extraction procedures for soil and sediment analysis—I. Standardization. *TrAC Trends Anal. Chem.* **1998**, *17*, 289–298. [CrossRef]
18. Zimmerman, A.J.; Weindorf, D.C. Heavy Metal and Trace Metal Analysis in Soil by Sequential Extraction: A Review of Procedures. *Int. J. Anal. Chem.* **2010**, *2010*, 387803. [CrossRef] [PubMed]
19. Bartington Instruments. *Operation Manual for MS2 Magnetic Susceptibility System*. MS2B Dual-Frequency Sensor, Sections 6.5–6.9. Available online: https://gmw.com/wp-content/uploads/2019/03/MS2-OM0408.pdf (accessed on 25 October 2026).
20. Chang, Y.C.; Yeh, H.D. Optimum allocation for soil contamination investigations in Hsinchu, Taiwan, by double sampling. *Soil Sci. Soc. Am. J.* **2007**, *71*, 1585–1592. [CrossRef]
21. Aitchison, J. The statistical analysis of compositional data. *J. R. Stat. Soc. Ser. B (Methodol.)* **1982**, *44*, 139–160. [CrossRef]
22. Lovell, D.; Pawlowsky-Glahn, V.; Egozcue, J.J.; Marguerat, S.; Bähler, J. Proportionality: A valid alternative to correlation for relative data. *PLoS Comput. Biol.* **2015**, *11*, e1004075. [CrossRef] [PubMed]
23. Krause, A.; McMahan, H.B.; Guestrin, C.; Gupta, A. Robust submodular observation selection. *J. Mach. Learn. Res.* **2008**, *9*, 2761–2801.
24. Frančišković-Bilinski, S.; Cukrov, N.; Cukrov, N. Magnetic Susceptibility as a Proxy for Metal Enrichment in Karstic Estuarine Sediments: A Case Study on the Krka River, Croatia. *Environments* **2026**, *13*, 258. [CrossRef]
25. Yskak, A.; Kuanushbayev, S.; Bekmyrza, Z.; Irzhanov, Z.; Nugmanov, A.; Yermoldina, G.; Tokusheva, A.; Fominov, V.; Bulaev, A.; Lyanga, P.; et al. Soil Contamination Around an Iron Ore Mining and Beneficiation Complex in the Semiarid Zone of Northern Kazakhstan. *Environments* **2026**, *13*, 369. [CrossRef]
26. Hoffmann, V.; Knab, M.; Appel, E. Magnetic susceptibility mapping of roadside pollution. *J. Geochem. Explor.* **1999**, *66*, 313–326. [CrossRef]
27. Hanesch, M.; Scholger, R. Mapping of heavy metal loadings in soils by means of magnetic susceptibility measurements. *Environ. Geol.* **2002**, *42*, 857–870. [CrossRef]
28. Lu, S.G.; Bai, S.Q. Study on the correlation of magnetic properties and heavy metals content in urban soils of Hangzhou City, China. *J. Appl. Geophys.* **2006**, *60*, 1–12. [CrossRef]
29. Lu, S.G.; Bai, S.Q.; Xue, Q.F. Magnetic properties as indicators of heavy metals pollution in urban topsoils: A case study from the city of Luoyang, China. *Geophys. J. Int.* **2007**, *171*, 568–580. [CrossRef]
30. Hu, X.F.; Su, Y.; Ye, R.; Li, X.Q.; Zhang, G.L. Magnetic properties of the urban soils in Shanghai and their environmental implications. *CATENA* **2007**, *70*, 428–436. [CrossRef]
31. Gleyzes, C.; Tellier, S.; Astruc, M. Fractionation studies of trace elements in contaminated soils and sediments: A review of sequential extraction procedures. *TrAC Trends Anal. Chem.* **2002**, *21*, 451–467. [CrossRef]
32. *ISO 21226:2019*; Soil Quality—Guideline for the Screening of Soil Polluted with Toxic Elements Using Soil Magnetometry. International Standard, 1st ed. International Organization for Standardization: Geneva, Switzerland, 2019. Available online: https://www.iso.org/standard/70136.html (accessed on 8 November 2026).

Disclaimer/Publisher's Note: The statements, opinions and data contained in all publications are solely those of the individual author(s) and contributor(s) and not of MDPI and/or the editor(s). MDPI and/or the editor(s) disclaim responsibility for any injury to people or property resulting from any ideas, methods, instructions or products referred to in the content.